

Full length article

Quantification of the influence of increased pre-stretching on microstructure-strength relationships in the Al–Cu–Li alloy AA2195



B.I. Rodgers*, P.B. Prangnell

The University of Manchester, Manchester, M13 9PL, UK

ARTICLE INFO

Article history:

Received 16 September 2015

Received in revised form

5 February 2016

Accepted 7 February 2016

Available online 23 February 2016

Keywords:

Aluminium

 T_1 phase

Precipitation

Work hardening

Strengthening

ABSTRACT

The effect of increasing pre-stretching to higher levels, than are currently used in industrial practice, has been investigated on the strength, microstructure, and precipitation kinetics seen during artificial ageing an Al–Cu–Li alloy AA2195 – focussing on the behaviour of the main strengthening phase, T_1 . Increasing the pre-strain level, to the maximum obtainable before plastic instability (15%), resulted in an increase in the T8 yield strength to ~ 670 MPa with a corresponding reduction in ductility from ~11 to 7.5%. Microstructure data have been used to deconvolute and model the effects of increasing pre-strain on the main strengthening components that contribute to this large strength increase. The precipitation strengthening model proposed by Dorin et al. [1] has been successfully employed to calculate the strengthening contribution of the T_1 phase and the increase in strength due to strain hardening has been modelled using X-ray line broadening measurements of dislocation density, using the modified Williamson–Hall approach. Refinement of the T_1 phase was observed to continue to higher pre-strains than previously thought, but it is predicted that this leads to a reduction in the strengthening contribution from precipitation. In contrast a low level of recovery was observed during stretching, and artificial ageing, resulting in an increasing contribution from strain hardening with pre-strain. Thus, it is shown that increasing the pre-strain prior to ageing results in a reduction in the strengthening provided by the T_1 phase, in favour of an increase in the strain hardening contribution.

© 2016 Acta Materialia Inc. Published by Elsevier Ltd. This is an open access article under the CC BY license (<http://creativecommons.org/licenses/by/4.0/>).

1. Introduction

Third generation (Gen3) aluminium-lithium (Al–Li) alloys [2] are of great interest to the aerospace industry owing to a number of key benefits they offer over conventional aluminium (Al) alloys [3–5]. In particular, their lower density, excellent corrosion resistance, and combination of higher fatigue performance, high strength and toughness, can lead to significant weight savings. They also offer a cost advantage over CFRPs (Carbon Fibre Reinforced Polymers) which has led to Gen3 Al–Li alloys being increasingly substituted for conventional 2xxx and 7xxx series materials in new aircraft designs [6].

Previous generations of aluminium-lithium alloys contained a higher concentration of lithium (Li) and had a lower density than the new Gen3 alloys. However, these earlier alloys suffered from high anisotropy, lower toughness, and manufacturing issues,

associated with the high Li level and precipitation of the metastable δ' and coarser equilibrium Li containing phases, such as T_2 [3,5,7]. New Gen3 alloys typically contain lower Li levels of 1–1.8 wt.%, which suppresses δ' formation, and have chemistries designed to promote T_1 as the dominant strengthening phase. These developments have proved to be extremely effective in providing high strength without the deleterious effects seen in the previous generation [1,8–10].

The conventional manufacturing route for aluminium aerospace plate involves a stretching operation after solution heat treatment, to relieve the large residual stresses developed on quenching, during which the material is typically plastically strained between 2 and 5% [11]. In Gen3 alloys this stretching operation is also critical to obtain an optimum distribution of T_1 precipitates, which are dislocation nucleated. It has been widely shown that a small pre-strain prior to artificial ageing produces a uniform distribution of dislocations within the matrix, which act as heterogeneous nucleation sites for the T_1 phase [8–10]. This results in the nucleation of a fine homogeneous distribution of the T_1 phase throughout the material during artificial ageing, leading to exceptional mechanical

* Corresponding author.

E-mail addresses: benjamin.rodgers@postgrad.manchester.ac.uk (B.I. Rodgers), philip.prangnell@manchester.ac.uk (P.B. Prangnell).

performance [5,8,12,13]. Stretching also serves to accelerate matrix precipitation and thus avoid competition with grain boundary precipitation, which leads to a detrimental effect on toughness [14]. The exact nucleation mechanism is still under debate, but is known to involve prior segregation of Cu and Mg to dislocation lines [15].

The T_1 (Al_2CuLi) phase has been extensively studied and is known to form as very thin semi-coherent hexagonal plates with a $\{111\}_{\text{Al}}$ matrix habit plane [16–18]. T_1 precipitates have a particularly high aspect ratio and provide a greater hardening effect than the θ' phase, which forms as octagonal plates on $\{100\}_{\text{Al}}$ planes [8,19]. As it is dislocation nucleated, increasing the pre-strain increases the density of T_1 nucleation sites and the resultant finer precipitate distribution reduces the average diffusion field size, so the matrix is depleted of solute in a shorter timescale. This results in accelerated ageing kinetics with increasing values of pre-strain. However, the benefits of stretching have been widely reported to saturate at pre-strains of around 6–9% in Al–Cu–Li alloys [8,9].

The T_1 plates were originally thought to be shear resistant [20]. In contrast, recent research by Deschamps et al. [1,21] has demonstrated that T_1 precipitates are cut by dislocations during plastic deformation, across the entire range of conventional ageing treatments, as the plates are very thin (~1.3 nm) and their thickness is very stable with ageing time at temperatures below ~170 °C [21–23]. Dorin et al. have proposed a strengthening model for the T_1 phase, based on earlier work of Nie and Muddle [24], that considers the interfacial and stacking fault energy contributions to a $\{111\}_{\text{Al}}$ habit plane, plate-shaped, precipitate's shear resistance. This model has been demonstrated to be able to reliably predict the yield strength contribution of the T_1 phase in a 2198 alloy for a wide range of plate dimensions and densities [1]. However, in this work, although it was reported that after ageing the alloy's yield stress was relatively constant for pre-strains greater than about 2% [1], the contribution of dislocation forest strengthening to the alloy's yield stress was not explicitly measured. It was also proposed that after recovery the residual strain hardening caused by pre-stretching compensates for a predicted reduction in precipitate strengthening, due to the reduced plate diameter that results from an increase in precipitate density with rising levels of pre-strain, and there is thus a coincidental linear correlation between strength and particle volume fraction in this alloy system.

Recent developments in rolling control technology can enable the production of plates with variable thickness that offer potential benefits in the production of nearer-to-net-shape sections; for example in the manufacture of tapered wing skins. One significant implication of applying this processing technology is the subsequent impact on the required stretching operation. The stretching of a tapered plate results in a strain gradient and for Al–Cu–Li alloys the maximum strain that can be achieved without tensile fracture limits the taper that can be utilised without omitting the critical stretching step. It is therefore important to better understand the impact of increasing plastic pre-strains, to near the plastic limit, on the peak-aged microstructure found in Gen3 plates and ultimately how this impacts on the materials peak yield strength and other mechanical properties.

While much prior work has been carried out to investigate the effects of increasing pre-strain on precipitation strengthening in Al–Li alloys within standard limits, there has been less published on the effects of more extreme stretching operations. The work presented here thus aims to examine the effect of increasing tensile pre-strains, to near the tensile plastic limit, on a typical Gen3 Al–Li alloy's ageing kinetics, microstructure and yield strength. It is also considered that, according to classical theory, higher pre-strains should perhaps lead to dynamic recovery and the formation of a dislocation cell structures [25]. This, in turn, could potentially cause microstructural heterogeneity by affecting the distribution of the T_1

phase. The effect of thermal treatment during artificial ageing, on reducing the strain-hardening contribution to the materials strength by dislocation recovery, is also currently largely unknown. Ultimately, this could have a profound impact on the mechanical properties of the alloy and how the different strength contributions relate to the overall peak yield strength of the material.

The work presented here thus aims to examine the effect of increasing tensile pre-strains, to near the tensile plastic limit, on a typical Gen3 Al–Li alloy's ageing kinetics, microstructure and yield strength. To this end, tensile tests, hardness testing and Differential Scanning Calorimetry (DSC) have been employed to explore the effect of higher pre-strain (i.e. above 6%) on a AA2195 alloy's ageing kinetics and yield stress, while simultaneously utilising the modified Williamson–Hall X-ray diffraction (XRD) peak broadening analysis to measure the effect on the residual dislocation density. Transmission electron microscopy has also been used to determine the effect of the pre-strain on the dislocation structures and to quantify the dimensions and distribution of the T_1 phase. This data has then been utilised to model the different strengthening contributions that contribute to the alloy's measured yield strength, as a function of the level of pre-strain applied prior to artificial ageing.

2. Experimental method

A typical Gen3 Al–Cu–Li alloy, AA2195, provided by Constellium Voreppe Research Centre in France, was used in this investigation. The alloy was supplied as 22 mm thick plate in a T841 temper. The composition range of AA2195 is provided in Table 1.

Tensile samples were cut from the 1/4 plate depth and machined in accordance with BS EN ISO 6892-1:2009 [26]. Each test sample was given a solution heat treatment (1 h at 510 °C) and water quenched. The majority of the samples were then naturally aged to a stable condition (24 h at room temperature; designated here as T4) before pre-straining, by tensile stretching, to plastic strain values ranging from 3 to 15%, (designated here as T3) and then being subjected to artificial ageing. The upper limit of 15% was selected after analysis of the work hardening rate in the T4 condition, which indicated that this was the maximum strain that could be reliably used while avoiding plastic instability. Some samples were also tensile tested immediately (within 10 min) after solution treatment and quenching (designated STQ).

Pre-stretching and tensile testing was carried out using an MTS Alliance RT/100 tensile machine at a strain rate of 2 mm/min, with the strain being monitored by a 25 mm clip gauge extensometer. The required plastic pre-strain values were produced by elongating the tensile samples in the T4 condition. Artificial ageing was performed with an initial heating ramp of 20 °C per hour, followed by an isothermal hold at 150 °C for a range of times up to 100 h. Following artificial ageing, the pre-stretched tensile samples were tested to failure to measure the effect of a pre-stretch on the material's tensile properties.

The effect of pre-strain on the ageing kinetics was first determined by measuring hardness curves, after applying varying degrees of pre-strain ranging from 3 to 15% to the T4 samples, using an Instron RT100 machine with a V044 indenter and a 0.5 Kg load. An average of five measurements was taken for each condition. Differential Scanning Calorimetry (DSC) analysis was also

Table 1
Nominal composition of AIRWARE alloy AA2195 (wt. %).

	Cu	Li	Mg	Zr	Mn	Ag	Al
Min.	3.70	0.80	0.25	0.08	—	0.25	Bal
Max.	4.30	1.20	0.80	0.16	0.25	0.60	Bal

performed, using a Netzsch – STA 449C Jupiter instrument, on samples subjected to varying degrees of pre-strain and at different stages through their artificial ageing treatment. This enabled the effect of pre-strain on the relative volume fraction of the T₁ phase to be determined from the integral of the T₁ precipitation exothermic peak in the DSC curves. The DSC samples were prepared by cutting slices from the gauge length of stretched tensile specimens using a Struers Minitom with a diamond cutting wheel. A baseline was measured using an annealed sample of pure aluminium and subsequently subtracted from the results obtained from each test sample. The DSC scans were carried out at a heating rate of 20 °C/min from 20 to 510 °C.

TEM samples were prepared by twin-jet electropolishing using a solution of 80% Methanol and 20% Nitric Acid at -30 °C and 14 V. Transmission Electron Microscopy (TEM) was employed to observe the effect of stretching on the dislocation structure using a Tecnai G2 T20 microscope operating at 200 kV. Scanning TEM (STEM), using a High Angle Annular Dark Field (HAADF) detector, was used to image the T₁ precipitates' size and spatial distribution. STEM imaging was conducted using an FEI Titan 80-200 FEG-TEM fitted with dual CEOS aberration correctors.

X-Ray Diffraction (XRD) was used to determine the effect of pre-strain on the dislocation density by the line broadening method [27]. Measurements were taken using a Rigaku Smartlab x-ray diffractometer equipped with a D/teX Ultra 250 detector. Data was collected using monochromatic Cu K α radiation ($\lambda = 0.154$ nm), with 40 KV and 30 mA, over a 2 θ range of 30–100°. Incident beam optics included a 2.5° soller slit, 1 mm slit and 5 mm beam mask, while a 0.5° soller slit was applied for the receiving optic. The 1 mm slit removed unwanted parasitic scattering and the soller slits served to limit beam divergence. The primary beam was monochromatised using a double Ge (220) crystal monochromator tuned for the Cu K α_1 line, so that the Cu K α_2 component was completely suppressed. The diffraction peaks were fitted with the program Fityk, employing the Pseudo-Voigt peak function and utilising a Levenberg–Marquardt algorithm to obtain the best fit [28]. The method employed to extract the dislocation density measurements from this data is discussed further below.

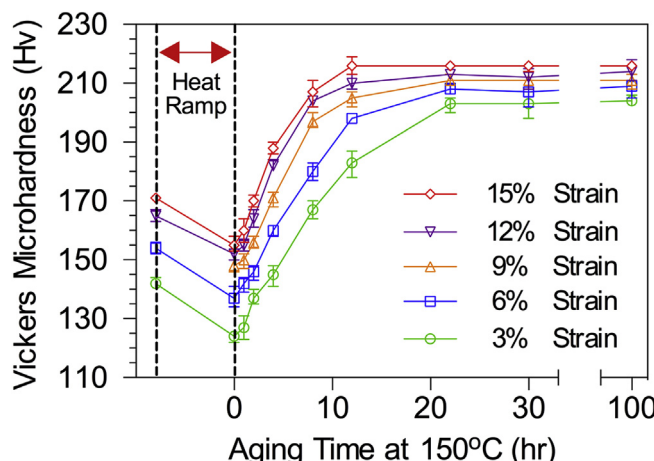


Fig. 1. Age hardening curves as a function of increasing pre-stretch, including the initial T3 hardness and heating ramp.

3. Results

3.1. Effect of pre-strain on the ageing kinetics

3.1.1. Age hardening curves

In Fig. 1 age hardening curves are compared, as a function of increasing pre-stretch up to 15%, on heat-treating the 2195 alloy at 150 °C for up to 100 h. These results demonstrate that increasing the pre-strain increased the hardness of the material both in the T3 and T8 tempers, but the effect appears less pronounced after artificial ageing. Fig. 1 further shows a similar level of softening occurring for each pre-stretch condition, during the initial heating ramp, owing to the reversion of solute clusters produced by natural ageing [19] and an expected increase in ageing kinetics with increasing level of pre-strain [8,9]. However, it can also be seen that, in contrast to some previous reports (e.g. Ref. [9]), the ageing kinetics and peak hardness achieved continues to increase into the higher pre-stretching regime, albeit at a reducing rate. It can further be observed from Fig. 1 that the peak hardness of the pre-strained samples all exhibited a maximum plateau region that remained stable when they were artificially aged for up to 100 h.

3.1.2. Volume fraction of the T₁ phase during ageing

The increase in relative volume fraction of the T₁ phase was tracked during artificial ageing by integration of the T₁ exothermic precipitation peak area in the DSC curves. As outlined by Dorin et al. [29], this is a reliable approach because in this alloy there is a well-defined exothermic peak in the DSC curves and when stretched the T₁ phase dominates the precipitate sequence. An example data set is provided in Fig. 2 (a) for samples subjected to a 3% pre-strain and aged at 150 °C for increasing times, between 0 h (end of the heating ramp) and 22 h (peak aged). Just below 300 °C an exothermic peak can be seen caused by precipitation of the single layer T₁ phase [30]. As the samples undergo artificial ageing the peak area can be seen to diminish, due to the increasing volume fraction of T₁ precipitates present prior to performing the DSC scan. Normalisation of the integrated area of the T₁ exothermic peak in each sample, relative to the 0 h case for the same pre-stretch, can therefore be used to determine the relative volume fraction of the T₁ phase at a given ageing time. Fig. 2(b) shows the corresponding evolution of the relative volume fraction of the T₁ phase, determined by this approach, in the 3% stretched example. The same analysis was subsequently repeated for all the samples with pre-strain values ranging from 3 to 15% (see Fig. 3). In each case the experimental points were fitted using the Avrami (JMAK) law [31] given by:

$$f_V = 1 - \exp(-Kt^n) \quad (1)$$

Where; f_V is the transformed volume fraction, t is the ageing time and K and n are constants.

In Fig. 3, JMAK curves, fitted to DSC data following the procedure described above, have been plotted on the same graph for increasing levels of pre-strain. These curves again demonstrate an increase in the ageing kinetics with rising levels of pre-strain. In agreement with the hardness curves in Fig. 1, it can be seen that the rate of acceleration diminishes as the pre-strain value increases into the higher pre-stretching regime and for pre-strain values above 10% there is little difference in the curves.

3.2. Effect of pre-strain on microstructure

3.2.1. Dislocation structures

The TEM images in Fig. 4 show the high dislocation densities seen in the AA2195 alloy in the solution treated and stretched T3 condition, in regions of similar thickness, after applying pre-strains

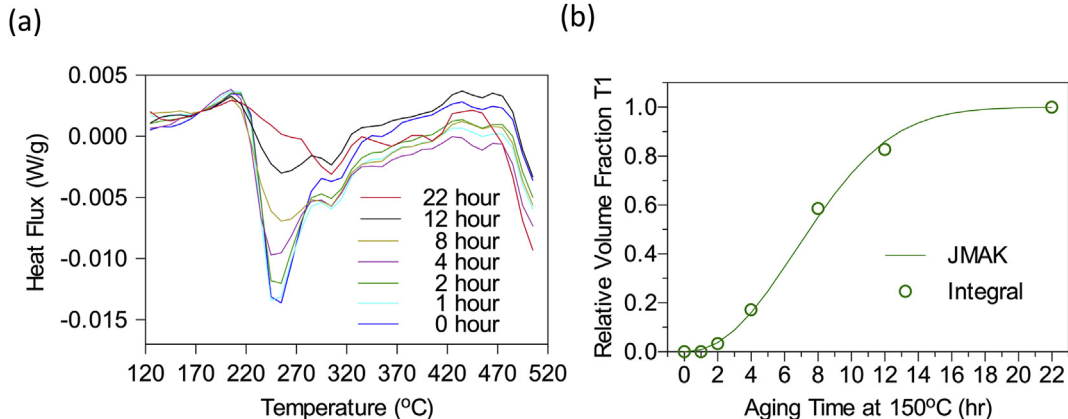


Fig. 2. (a) Example DSC curves for the 3% pre-strain condition T3, with increasing ageing times at 150 °C, showing the T₁ precipitation exotherm in the temperature range 200–300 °C and (b) the evolution of the relative volume fraction of the T₁ phase as a function of ageing time, determined by integration of the precipitation exotherm peak area.

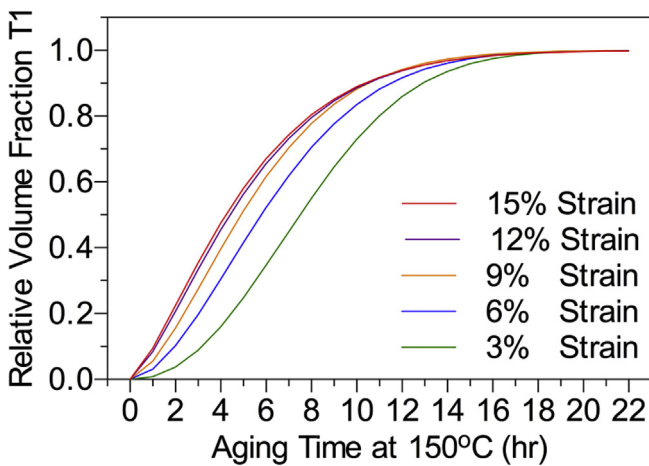


Fig. 3. Fitted JMAK curves showing the evolution of the relative volume fractions of the T₁ phase, as a function of ageing time at 150 °C, with pre-strain values ranging from 3 to 15%.

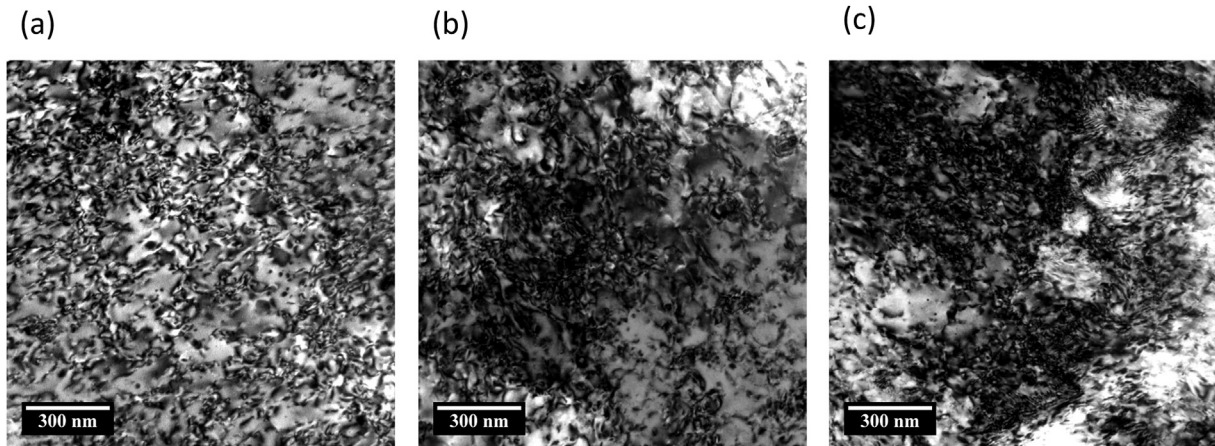


Fig. 4. Bright field TEM Images showing the uniform dislocation density seen in the AA2195 alloy following pre-strains of (a) 3%, (b) 9% and (c) 15%.

of 3, 9 and 15%. At this magnification the images reveal a uniform, but increasing, density of dislocations in dense forests throughout the aluminium matrix with rising levels of pre-strain. Both high angular resolution EBSD and systematic tilting were used on the

samples with the highest pre-strain, to investigate the possibility of the formation of cell structures. In Fig. 5 a bright field tilt series, with a two beam condition, is provided at a lower magnification from the sample with the highest pre-strain of 15%. This again shows a uniform dislocation density and that there is little evidence of cell formation. Although some recovery would be expected in pure aluminium at this strain level [32], it can be noted that in the alloy studied this appears to have been retarded. Overall, the dislocation structures are similar to those found in high Mg content Al alloys at this strain level, where solute has a strong effect on inhibiting recovery [33].

3.2.2. Dislocation density measurements

Because it is extremely difficult to reliably measure the high dislocation densities shown in Fig. 5 by TEM after artificial ageing, when dislocations are masked by precipitate coherency contrast, x-ray diffraction peak-broadening analysis was utilised to complement the qualitative TEM observations. According to the work of Ungar [34,35], diffraction peak broadening can be reliably correlated to the dislocation density within a crystalline material when

the dislocations are reasonably abundant (density values larger than $5 \times 10^{12} \text{ m}^{-2}$) and uniformly distributed in forests, as was the case in the alloy investigated here (Fig. 4). It should also be noted that peak broadening also occurs when crystallites smaller than

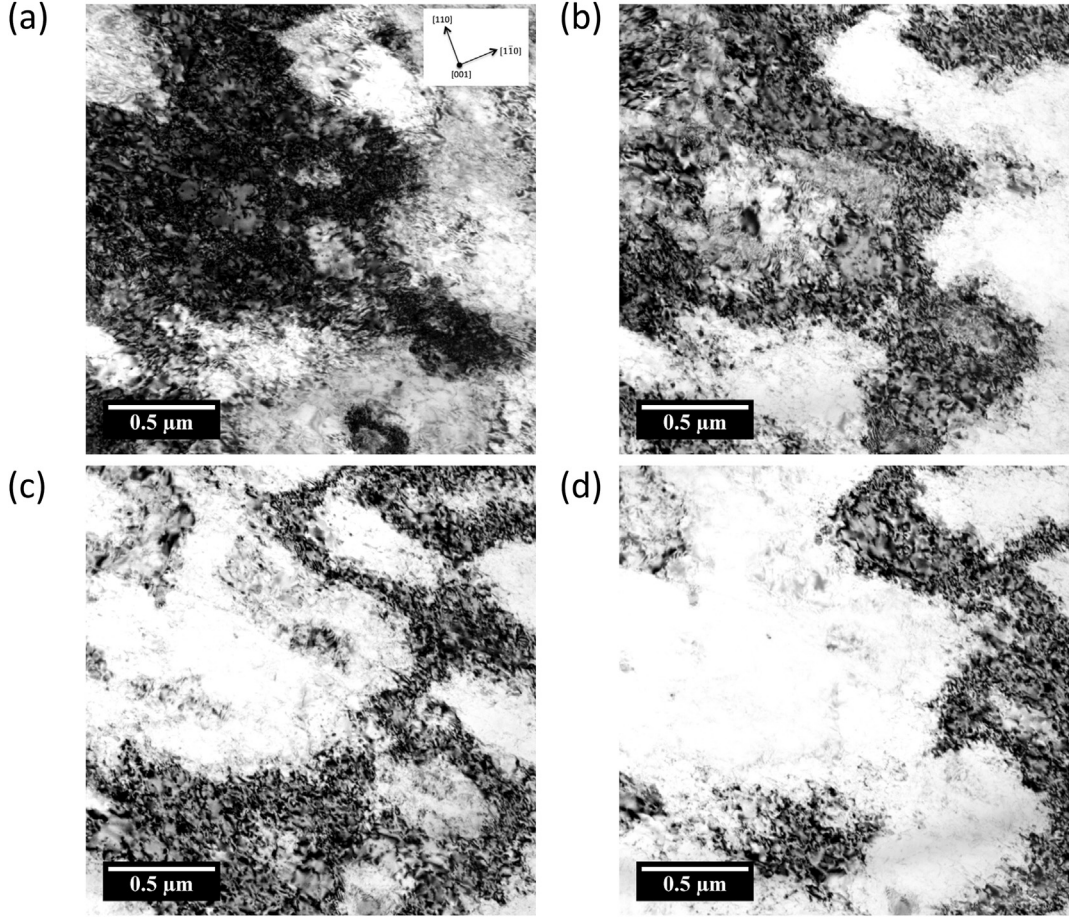


Fig. 5. Bright field TEM two beam condition tilt series of the dislocation structure in AA2195 after a 15% Pre-Strain; (a) 0° (b) 2° (c) 4° (d) 6° tilt around $[1\bar{1}0]$.

$\sim 1 \mu\text{m}$ are present, which is known as size broadening. However, in this instance, due to the large grain size ($50 \mu\text{m}$) and the absence of cell formation in the T3 samples we can be confident in attributing any peak broadening exclusively to an increase in the dislocation density.

A high resolution 2θ scan of the {111}, {200}, {220} and {311} diffraction peaks was performed (using continuous scanning at a rate of $0.2^\circ/\text{minute}$) to measure the effect of increasing pre-strain on peak broadening, in both the pre-stretched and artificially aged conditions. A Pseudo-Voigt function was subsequently fitted to each diffraction peak in order to calculate the FWHM. The experiment presented used very high-resolution optics to produce a highly collimated and monochromatic x-ray beam. Therefore, any instrumental peak broadening can be considered negligible [36].

Dislocation density values were subsequently calculated using the Modified Williamson–Hall plot (Fig. 6), to fit ΔK as a linear function, using the relationship [34]:

$$\Delta K = (0.9/D) + \left(\frac{\pi Mb^2}{2}\right) \rho^{1/2} K^2 \bar{C}_{hkl} \quad (2)$$

Where ΔK is the strain broadened FWHM in reciprocal space given by:

$$\Delta K = \frac{2 \cos \theta \cdot \Delta \theta}{\lambda} \quad (3)$$

Where θ is the diffraction angle, λ is the wavelength of the x-rays, D is the crystallite size, M is the Wilkens arrangement parameter, b is

the burgers vector (0.286 nm for Aluminium), ρ is the dislocation density and K is the diffraction vector defined by:

$$K = \frac{2 \sin \theta}{\lambda} \quad (4)$$

Where \bar{C}_{hkl} is the average contrast factor for each specific plane hkl .

The differences in the average contrast factors (\bar{C}_{hkl}) for different diffraction peaks, are used to account for broadening anisotropy [37,38], by:

$$\bar{C}_{hkl} = \bar{C}_{h00} (1 - qH^2) \quad (5)$$

$$\text{Where : } H^2 = \frac{h^2 k^2 + h^2 l^2 + k^2 l^2}{h^2 + k^2 + l^2} \quad (6)$$

Where q represents different broadening anisotropies and varies depending on whether dislocations are edge or screw in character [37,38]. As such, the value of \bar{C}_{hkl} can vary significantly between edge and screw dislocations. We have assumed in this instance that there is an even distribution of both edge and screw dislocations and so an average value for \bar{C}_{hkl} has been taken. We have also assumed that the dislocation microstructure is the same in all grains and that the contrast factor is the only cause of broadening anisotropy. In light of recent research, it should be considered that small systematic errors may exist due to this simplified approach [39]. These errors can be reduced using the plasticity approach to calculating contrast factors, which assumes

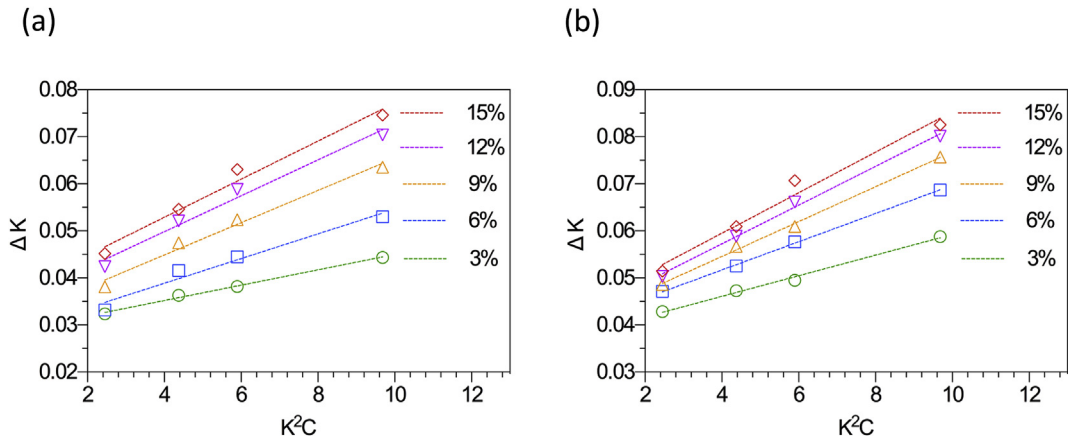


Fig. 6. Modified Williamson–Hall Plots for (a) T3 condition (b) T8 condition.

that different grains have different dislocation populations, which are calculated using a polycrystal plasticity model [39]. However, for the purposes of this research reasonable estimates of the dislocation density can be made by the simplified homogeneous approach (Eq. (5)) to calculating contrast factors [37]. The software package ANIZC was utilised to calculate the required average contrast factors [40].

The resultant Modified Williamson–Hall Plots can be seen in Fig. 6, and show good fit to the ideal linear behaviour. The effective dislocation densities calculated by this method are plotted against the level of pre-strain, for both the T3 and T8 aged samples, in Fig. 7. The results reveal a near-linear increase in dislocation density with increasing pre-strain, until the highest pre-strain value used (15%), which demonstrates a low level of recovery during pre-straining at room temperature to comparatively high strain levels in this alloy.

Surprisingly, after artificial ageing, the x-ray data showed a slight increase in the FWHM for each diffraction peak, giving an increase in ΔK , which resulted in a uniform systematic increase in the ‘apparent’ calculated dislocation density values, across all pre-strain levels. It has been previously reported that, typically, precipitation does not have an effect on line broadening [35]. However, in the T8 temper the 2195 alloy contains the semi-coherent T_1 phase, which form almost exclusively on dislocations. These

precipitates generate matrix coherency strains which are known to increase peak broadening, although dislocations are typically considered to be the dominant lattice defect and therefore the major component effecting peak width [35,41]. Therefore, it would seem reasonable to suggest that the small increase in ‘apparent dislocation’ density seen in Fig. 7, after ageing, can be attributed to the introduction of matrix coherency strains associated with the formation of a constant volume fraction of the T_1 phase, combined with a low level of recovery occurring on artificial ageing; i.e. the uniform increase in ‘apparent’ dislocation density observed, suggests minimal static recovery during the ageing heat treatment, as this would be expected to reduce the dislocation density leading to a decrease in ΔK and occur at a greater rate the more highly strained the material.

3.2.3. Distribution and size of the T_1 phase

STEM-HAADF imaging was used in order to characterise the size and distribution of the T_1 precipitates after ageing to the T8 condition. This method is preferable to bright field TEM imaging as it removes unwanted diffraction contrast and enabled more accurate measurements of the T_1 plate dimensions. Examples of STEM-HAADF images of the T_1 phase seen in the peak aged samples with increasing levels of pre-strain are shown in Fig. 8, taken close to a $<110>_{Al}$ zone axis. Qualitatively, it is apparent from these images that there is a reduction in the T_1 plate diameter with the level of prior-plastic strain. An additional low magnification image is provided in Fig. 9, to illustrate the exceptionally uniform distribution of the T_1 phase that was still seen in the sample subjected to the highest pre-strain level of 15%. Higher magnification images in Fig. 10 confirm the thin dimensions of the T_1 phase and show the presence of only a minor fraction of θ' precipitates within the aged material.

Measurements of the T_1 plates’ size distributions (from at least 200 precipitates in several sample areas) were made manually from STEM-HAADF images using ImageJ image processing software with increasing pre-strain (Fig. 11 (a–c)). These results demonstrate a decrease in the width of the precipitate diameter frequency distributions with increasing pre-strain, suggesting an increase in the homogeneity of the distribution of the T_1 precipitates. Results for the average plate diameter in Fig. 11 (d) also show a continued reduction in size with increasing pre-strain up to the maximum value used of 15%. In line with previous studies [1,8], high resolution TEM imaging further confirmed that the thickness of the T_1 plates remained effectively constant at approximately 1.3 nm, in all the samples examined (e.g. Fig. 10 (a)).

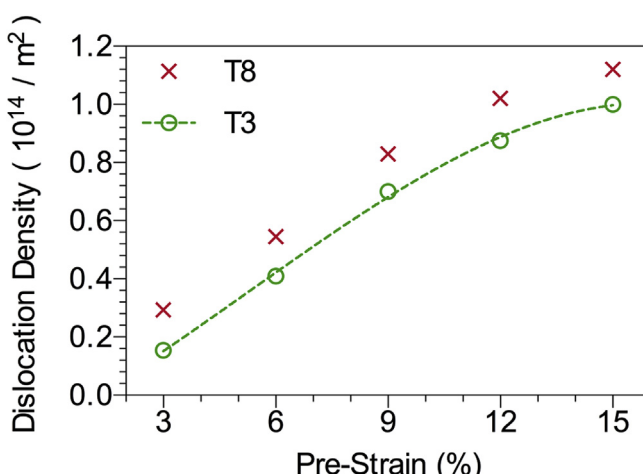


Fig. 7. Effective dislocation density measurements obtained by the Modified Williamson–Hall method, showing the estimated dislocation density as a function of pre-strain for samples in both the T3 (solution treated and stretched) and T8 (22 h at 150 °C) conditions.

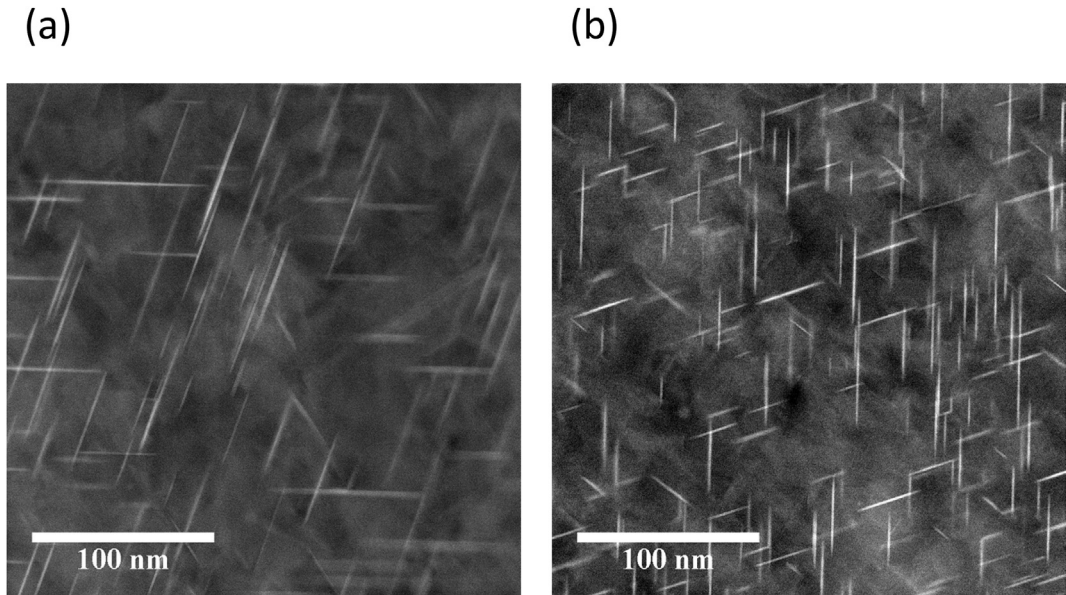


Fig. 8. STEM HAADF images showing T1 precipitates seen in AA2195 in the T8 condition (close to the $<110>_{\text{Al}}$ zone axis) for (a) 3% and (b) 15% Pre-Strain.

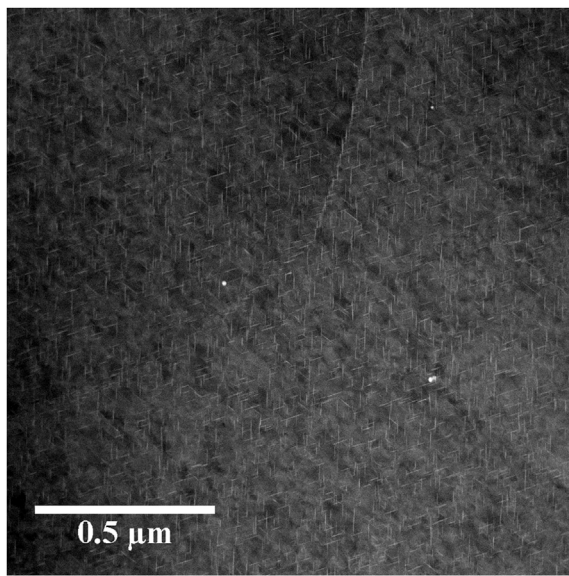


Fig. 9. STEM HAADF image showing the uniform distribution of the T₁ phase seen in the peak aged AA2195 alloy following a 15% pre-strain ($<110>_{\text{Al}}$ Zone Axis).

By assuming a constant peak volume fraction in the peak aged condition (Fig. 3) [1,9] and a constant plate thickness, the number density of the T₁ phase could be evaluated from Refs. [11];

$$N = \frac{4f_v}{\pi t D^2} \quad (7)$$

Where; t is the average plate thickness, D is the average plate diameter and f_v is the volume fraction.

The resultant calculated precipitate number densities are plotted in Fig. 11 (d) and demonstrate a corresponding increase in number density as the average precipitate diameter reduces with level of pre-strain.

In addition to the STEM observations, further information can be garnered from the fitted Avrami curves shown in Fig. 3. It has been

shown theoretically that the value of the Avrami exponent (Eq. (1)) can elucidate changes in the nucleation mechanism, or homogeneity and morphology of precipitate phases [42,43]. In Fig. 12 a systematic reduction in the value of the exponent (n) was seen with increasing pre-strain. In keeping with the STEM observations, this behaviour can be attributed to an increase in the homogeneity of the size distribution of the T₁ phase with a higher level of stretching prior to ageing.

3.3. The effect of high pre-stretching on the T8 yield stress

The average mechanical properties (from 3 tests) obtained from tensile testing the peak aged, pre-stretched, samples are summarised in Fig. 13. This reveals a significant increase in the peak yield stress of the material with increasing pre-strain, which continued into the higher pre-strain regime, from 590 MPa at a standard 3% stretch, to ultimately reach a maximum value of 668 MPa, with the greatest pre-stretch applied of 15%. The tensile strength also increased from 658 to 686 MPa over this pre-stretch range. However, this increase in strength led to a decrease in strain to failure from $\epsilon_f = 11\%$, for the conventional 3% level of pre-stretch, to $\epsilon_f = 7.5\%$, with a 15% pre-stretch.

4. Strength modelling

While there is merit in using more sophisticated flow stress superposition laws [44], following the work of Shercliffe and Ashby [45] and other authors [46,47], in the interest of simplicity, the main strengthening terms of interest can be summed by the following relationship;

$$\sigma_y = M(\tau_B + \Delta\tau_p + \Delta\tau_P) \quad (8)$$

Where; σ_y is the yield strength of the material, τ_B is the constant base shear strength, $\Delta\tau_p$, and, $\Delta\tau_P$, are the increase in strength due to strain hardening and precipitation, respectively, and M is the Taylor factor (usually assumed to be about 3.1 for a material with a relatively weak texture [48,49]).

The base strength of the solution treated alloy prior to pre-straining and ageing will result from a combination of the

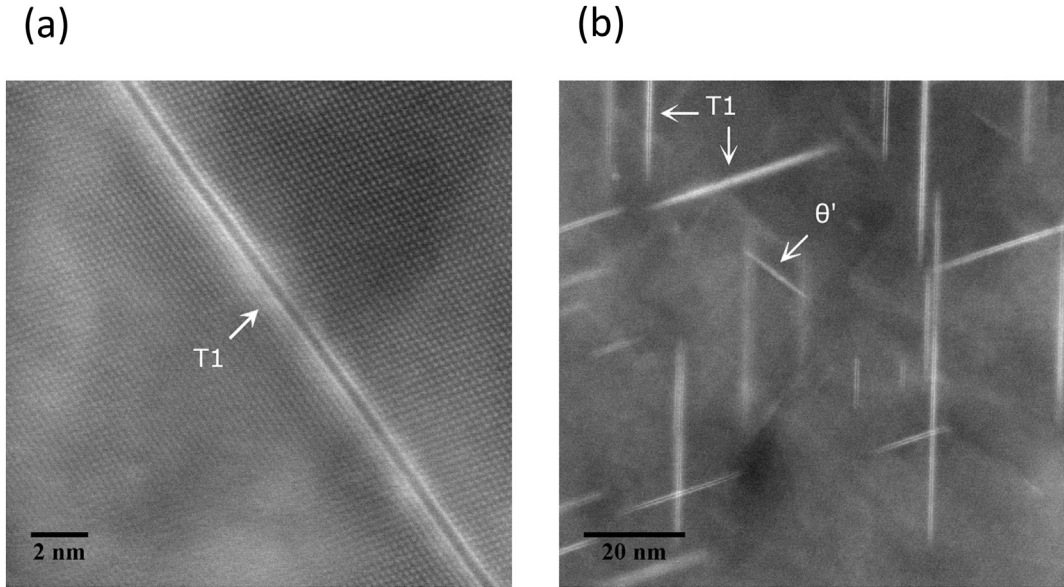


Fig. 10. STEM HAADF images of (a) a single T_1 plate and (b) an example of a θ' precipitate within the peak aged AA2195 subjected to a pre-strain of 15% ($<110>_{\text{Al}}$ zone axis).

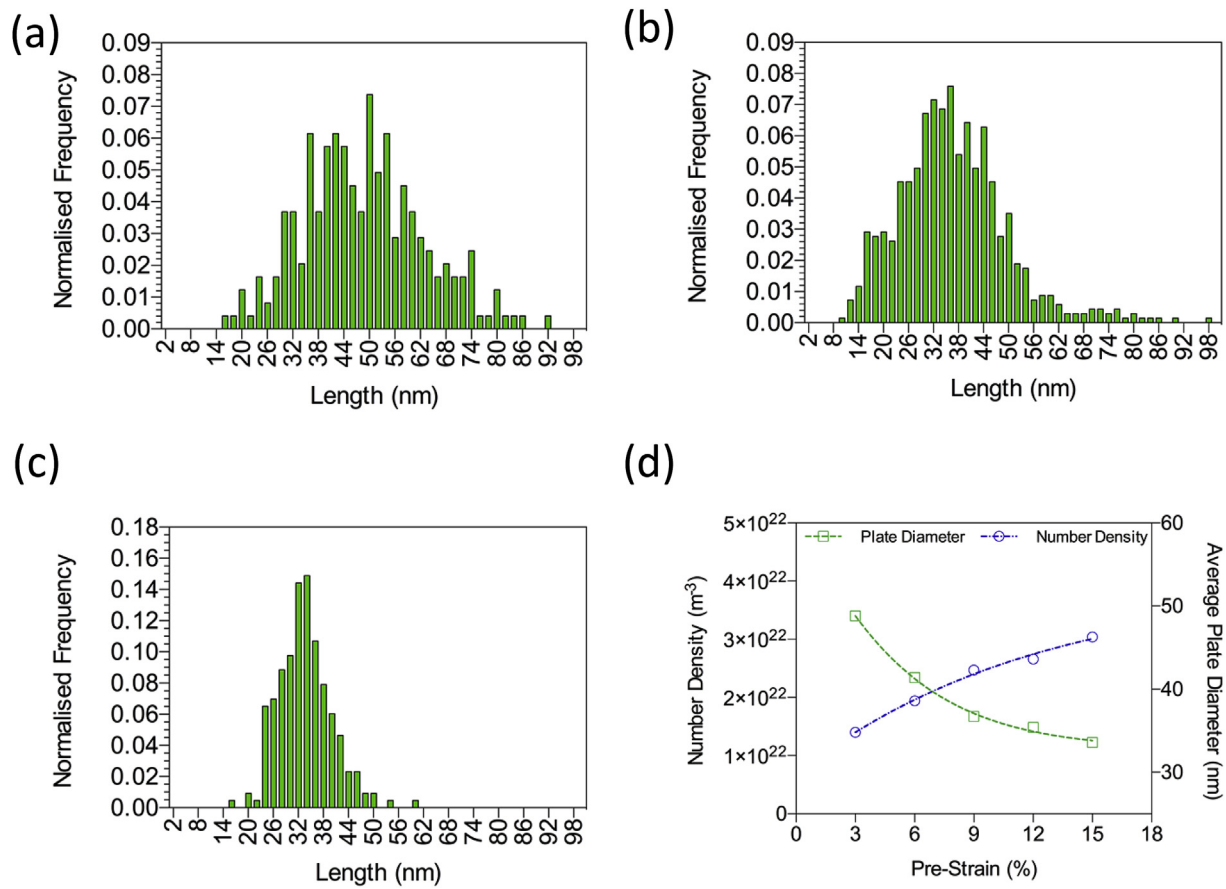


Fig. 11. Evolution of the mean T_1 plate diameter and size distribution for three pre-strain values; (a) 3%, (b) 9%, and (c) 15%, measured from HAADF-TEM images. (d) Evolution of the average plate diameter and calculated number density with increasing pre-strain.

intrinsic shear resistance of the lattice (τ_i) and solid solution strengthening (τ_{ss}). Recent research has demonstrated that a significant amount of Cu often remains in solution after ageing [50,51]. Therefore, for the sake of simplicity, and following the approach of

other authors [1,52,53] it is assumed that to a first approximation this term will remain constant during age hardening, as any change from a loss of solid solution strengthening will be relatively small compared to the high strength increase from precipitation [54].

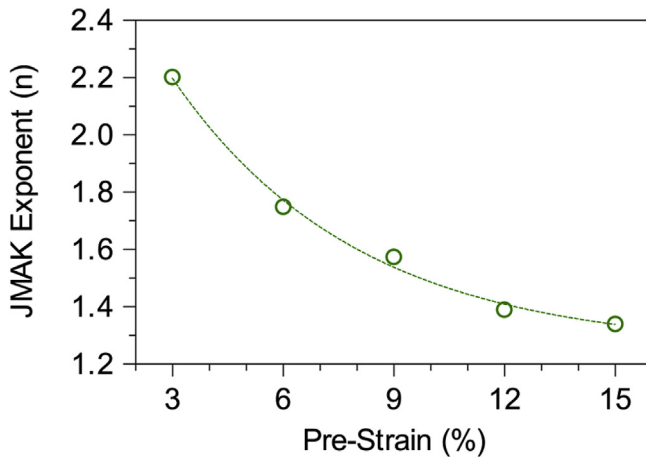


Fig. 12. Change in the JMAK exponent (n) with increasing pre-strain.

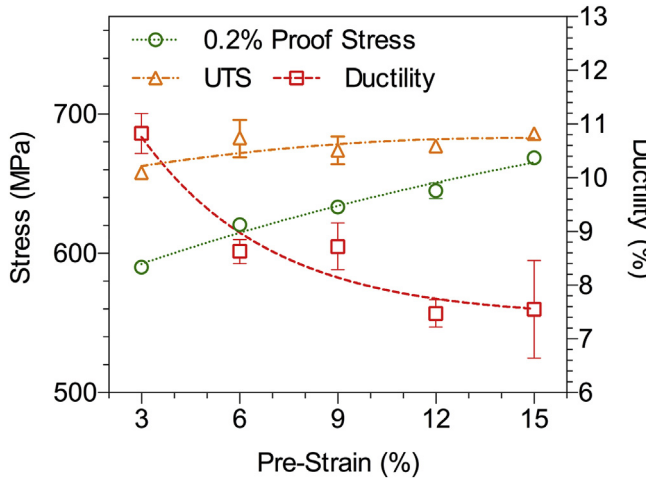


Fig. 13. Yield Stress (0.2% proof), tensile strength and ductility (plastic strain to failure) in the T8 Temper (22 h at 150 °C), plotted as a function of pre-Strain.

As the XRD peak broadening results imply little static recovery occurred during artificial ageing, it is reasonable as an upper bound to assume that any increase in the yield strength resulting from strain hardening will be largely retained in the peak-aged material. In the first instance, the upper bound strain hardening contribution can thus be determined using the increase in yield stress seen in the true stress–strain curve produced during tensile stretching of the T4 material. Any further increase in the yield stress in the T8 temper can then be attributed to precipitation of the main strengthening T_1 phase, which can be obtained by subtraction of the strain hardening contribution and base strength immediately after solution treatment from the total measured yield strength. The two main strengthening contributions can thus be separated using the tensile-stress strain data, as shown in Fig. 14. From this preliminary analysis it is apparent that the strengthening contribution from precipitation of the T_1 phase diminishes with increasing pre-strain. Indeed, at a maximum pre-strain value of 15% the strength increase from strain hardening is approximately equal to that from precipitation. This preliminary interpretation will be further justified below by modelling the individual strain and precipitation hardening contributions.

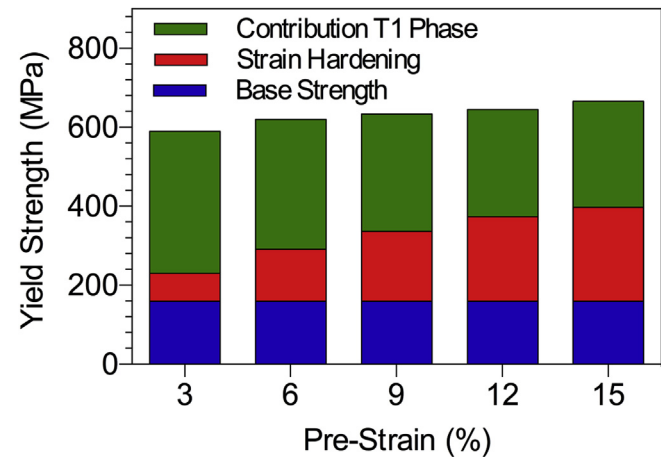


Fig. 14. Effect of Pre-Strain on the main components contributing to the yield strength in the T8 temper, as a function of pre-strain.

4.1. Calculation of the strain and precipitation hardening contributions

4.1.1. Strain hardening

In addition to the above approach, the measured dislocation density values obtained by XRD of the material following stretching in the T4 temper can be used to estimate the contribution from forest hardening to the yield strength of the material, before artificial ageing, from the standard expressions relating dislocation density to shear strength [11] given by:

$$\Delta\sigma_p = M\alpha\mu b\rho^{1/2} \quad (9)$$

Where; α is a dimensionless constant between 0.2 and 0.5 [55], μ is the shear modulus, b is the burgers vector ($\approx 0.286 \text{ nm}$ for Al), and ρ is the dislocation density.

In Fig. 15 (a) it can be seen that, when the measured dislocation densities from Fig. 7 are used with Eq. (9), the predicted increase in yield stress from strain hardening gives a very reasonable agreement with the experimentally determined stress–strain curve for a T4 temper tensile sample, with a fitted value of $\alpha = 0.3$. If the lower base strength is taken into account, a good fit can also be obtained with a sample that was tested immediately following solution treatment (STQ condition), with no adjustment to α .

4.1.2. Precipitation hardening

Recent literature has demonstrated the efficacy of a model originally developed by Nie and Muddle [24], and subsequently validated by Dorin et al. [1], for predicting the strengthening contribution of the thin shearable T_1 plates. The model is based on the assumption of (Friedel) statistical interactions between a dislocation and weak obstacles, where the obstacle strength is controlled by the increase in interfacial energy on shearing a precipitate and has previously been validated against TEM and SAXS measurements of the precipitate size distribution [1,24]. The thin disc geometry of the T_1 precipitates, with respect to their $\{111\}_{\text{Al}}$ habit plane and the $\langle 001 \rangle_{\text{Al}}$ shear direction, is explicitly considered by Dorin et al. [1], who also included a stacking fault energy term, giving:

$$\Delta\tau_p = \frac{1.211D\gamma_{\text{eff}}^{3/2}}{t^2} \sqrt{\frac{bf_v}{\Gamma}} \quad (10)$$

Where; $\Delta\tau_p$ is the increase in the critical resolved shear stress due to precipitation, D is the average precipitate diameter, t is the

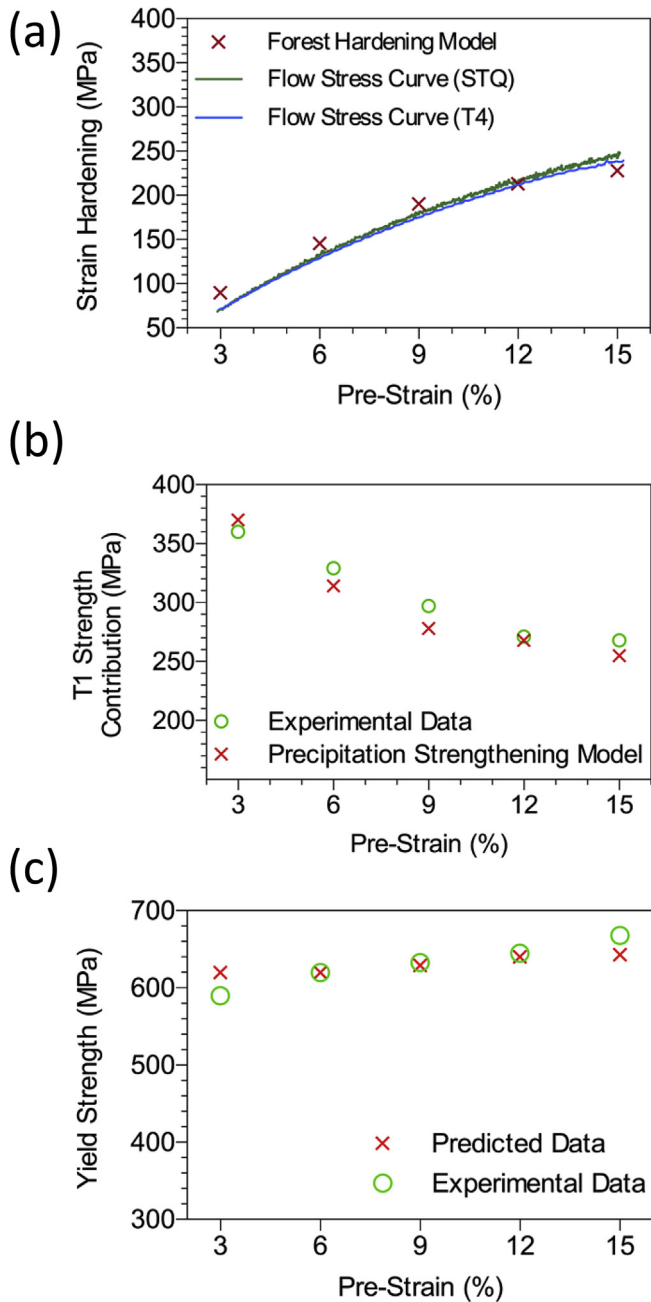


Fig. 15. Comparison of the calculated contributions to yield strength from strain and precipitation hardening; (a) the increase in strain hardening predicted by Eq. (9), using dislocation densities measured by XRD, compared to tensile stress strain curves for samples in the STQ and T4 condition, (b) the contribution from precipitation of the T_1 phase using Eq. (10), with data measured by TEM, compared to the expected yield strength if the upper bound effect of strain hardening is deducted (e.g. (a)). In (c) the predicted contributions are combined and compared to the effect of pre-strain on the measured tensile yield stress in the T8 temper.

thickness, and γ_{eff} is an effective interfacial energy term that considers both the interfacial and stacking fault energy contributions associated with shearing a precipitate. The other terms have their usual meaning; b is the Burgers vector (≈ 0.286 nm for Al), f_v is the volume fraction of the T_1 phase, and Γ is the dislocation line tension. It should be noted that this model is only applicable for T_1 strengthened alloys in the under-aged and peak aged conditions and if substantial over-ageing occurs Orowan by-passing would need to be considered. However, for the conditions studied here,

where the plates did not thicken during ageing, this would not be of concern [1].

In Fig. 3 it is apparent that the peak volume fraction of the T_1 phase is constant for ageing times in the peak aged plateau hardness region (Fig. 1) and it has also been shown to remain unchanged with increased levels of pre-strain, which does not affect the level of solute retained in solution at equilibrium [1,9]. Therefore, a reliable value of volume fraction can be taken from the literature for an alloy with a similar composition of $f_v = 3.4\%$ [1]. The precipitate interfacial energy term γ_{eff} is thus the only adjustable parameter in Eq. (10). It has previously been fitted to data for the T_1 phase by Dorin et al. [1], who obtained a value of $\gamma_{eff} = 0.107 \text{ J m}^{-2}$. Using these parameters, and the simple superposition law (Eq. (8)) if the upper bound effect of strain hardening is first deducted, by using the T3 data for dislocation density in Fig. 15(a) and assuming no recovery on artificial ageing, a good fit to the experimentally determined yield stress contribution from the T_1 phase was obtained, despite the simplified approach, as can be seen in Fig. 15(b) and (c).

5. Discussion

When viewed overall, the results show that increasing the pre-strain applied prior to ageing, beyond levels normally used in industrial practice, has a more significant effect than formerly thought on the microstructure and strength of a typical Gen3 Al–Li alloy. For example, previous research has commonly suggested that the microstructure refinement benefits of pre-stretching tend to saturate at strain levels above about 6% [8,9], whereas the density of the T_1 phase was seen here to still increase at higher strain levels. The DSC results (Fig. 3) also showed that acceleration of T_1 precipitation kinetics continued for pre-stretching above 6%, albeit at a rapidly diminishing rate. However, although the kinetics did not change significantly for pre-strains above about 10%, there was still a continual increase in yield stress (Fig. 13) and in the T8 condition this led to a remarkably high strength that approached 700 MPa at the maximum pre-strain of 15%.

An important factor in the effect of pre-straining on the T_1 phase, and its role in precipitation hardening, is the clear influence this has on the dislocation nucleation site density in the material prior to artificial ageing [13]. During ageing treatments in aluminium aerospace alloys, pre-stretching is normally thought to increase the effectiveness of precipitation hardening by refining the particle size distribution, as second phase precipitation dominates the materials strength and significant recovery is usually expected [8,56]. However, as will be discussed further below, strain hardening was found to have a larger direct effect on the yield strength after artificial ageing than anticipated.

In the AA2195 alloy studied, a very uniform distribution of dislocations was still seen at high pre-strain levels, in the form of dense tangled forests (Figs. 4 and 5). In addition, the XRD analysis of the dislocation density indicated a low level of recovery during both stretching and subsequent artificial ageing, across the full range of pre-strain values investigated. In the first case, this can be inferred from the slow rate of reduction in the rate of increase in dislocation density with pre-straining, which increased nearly linearly with strain in Fig. 7. In the second case it can be inferred from the fact there was a small uniform increase in the FWHM of the Al matrix diffraction peak profiles across all the pre-stretched samples after the ageing heat treatment, rather than a reduction that increased with increasing initial dislocation density (Fig. 6). This behaviour can thus be attributed to the development of coherency strains during precipitation of the semi-coherent T_1 phase, combined with a low level of recovery; i.e. a slight, constant, increase in line broadening after artificial ageing across all pre-strain

levels is consistent with an increase in coherency strains from precipitation of a constant volume fraction of the T₁ phase and inconsistent with increasing levels of pre-strain driving higher levels of recovery during artificial ageing. In addition, when an upper bound contribution for forest hardening was predicted from stretching, based on dislocation densities obtained prior to ageing and combined with the precipitation hardening model proposed by Dorin et al. [1], using previously verified values for the only independent fitting parameters, this also gave good predictions for the strength of the material in the T8 temper (Fig. 15 (c)). The TEM images, XRD data and modelling results are thus self-consistent with the supposition that limited recovery took place, either dynamically during stretching, or statically, during the thermal treatment involved in artificial ageing.

This low level of recovery is important, in that it has a significant influence on the material's strength in the T8 temper at high pre-stretch levels and suggests strong solute interactions occur with dislocations in the alloy studied. Mg has long been known to greatly inhibit recovery in Al-alloys [25,57] and the images of the dislocation forests shown in Figs. 4 and 5 are extremely similar to those seen in non-heat treatable Al–Mg alloys deformed to equivalent strains that have Mg levels of over 5 wt.% [33]. Mg has often been associated with a reduction in the stacking fault energy (SFE) in Al, which in turn restricts cross slip. However, its main effect, on inhibiting recovery and dislocation cell formation, is from the drag of solute atmospheres and the thermal activation of solute atoms away from climbing dislocation jogs [33,58]. In the current material the Mg level was less than 1 wt%, so such a strong effect would not be expected from this element, but the Cu content in AA2195 is around 4 wt%. Relative to Mg, the influence of Cu on recovery in Al solid solutions has historically received less attention. While Cu increases the SFE [59], when compared at the same atomic concentration, it has been found to have a greater influence on both solid solution strengthening and reducing the rate of recovery [33,54]. Furthermore, recent atom probe studies have shown clear evidence of Mg and Cu segregation to dislocations in the early stages of ageing [15]. In Al–Cu–Li–Mg alloys the nucleation of the T₁ phase on dislocations has now been well documented [8–10]. Thus, it is highly likely that the ageing process has a powerful effect on inhibiting recovery of dislocation structures in an alloy where there is such a strong association between age hardening and dislocation assisted nucleation.

The increase in dislocation density with pre strain was found to continue to affect the precipitate size and size distribution of the T₁ phase, with respect to the plate diameter to high pre-strain levels. Measurements from STEM images (Fig. 11) demonstrated a continued decrease in the T₁ plate's average diameter, as well as a reduction in the spread in their size distribution, and a corresponding increase in number density with increasing pre-strain levels above 9%. The spatial distribution of the T₁ phase was also found to reflect the high and uniform dislocation density seen in the samples subjected to large pre-strains and increased in density and homogeneity throughout the matrix even up to pre-strain levels of 15% (Fig. 9). The greater and more uniform nucleation site density provided by stretching to higher strain levels, thus led to a reduction in the diameter individual precipitates could grow to before solute was depleted from the surrounding matrix by overlap of neighbouring diffusion fields. The reduced variability in distance between nucleation sites, caused by a higher dislocation density, could be correlated to a reduction in the spread in the T₁ plates' size distribution with higher levels of pre-stretching, and in addition this has been shown to lead to a reduction in the JMAK exponent, n, with increased pre-strain (Fig. 12).

In contrast, the thickness of the T₁ plates remained constant (at approximately 1.3 nm) with increasing pre-strain values across the

entire stretching range. Previous investigations have shown that at standard artificial ageing temperatures (i.e. 155 °C), once nucleated, the thickness of the T₁ phase remains constant at a single minimum structural unit high for extremely long ageing times, owing to the difficulty of ledge nucleation [1,19]. T₁ plate thickening has only been observed to occur at higher ageing temperatures (e.g. 190 °C) through the nucleation of new growth ledges which add four new atomic layers as they progress across the broad faces of the plate [1,60,61].

The predictions plotted in Fig. 15 showed that the thin plate precipitation hardening model, originally proposed by Nie and Muddle [24], gave predictions for the effect of pre-strain on the increase in T8 yield stress that were consistent with the experimental data, if the upper bound contribution of strain hardening is first deducted. In applying this model, all the precipitate parameters were measured directly from HAADF-TEM images, apart from volume fraction and the effective interfacial energy, which were taken from the work of Dorin et al., where the model has been previously independently validated [1]. However, irrespective of how the forest hardening term contributes to the T8 yield strength, it is very apparent from Fig. 15 (b) that the strengthening contribution from precipitation is predicted to reduce with increasing pre-strain in the high strain range investigated (Fig. 15).

As pointed out by Dorin et al. [1], for most metallurgists it is counter-intuitive that in an age-hardening alloy refinement of the precipitate size distribution, by stretching, can lead to a reduction in the strength contribution from precipitation. However, for the T₁ phase this case has been well argued in their series of papers [1,18,19,21,30,62] and is a direct consequence of the thin nature of the T₁ precipitates, which leads them to be sheared by dislocations. The results presented here support this finding, in that when the effect of strain hardening is subtracted from the yield stress, it is very apparent that the strengthening contribution from precipitation reduces with increasing pre-strain in the high strain range investigated (Fig. 15). As discussed by Dorin et al. [1], this behaviour can be correlated to the reduction in diameter of the T₁ plates that occurs on increasing the level of stretching, which is caused by the increase in nucleation site density. With a constant plate thickness and volume fraction, this results in a higher number density of precipitates (Fig. 11 (d)), but with thin disc shaped particles the increase in statistical interactions with a dislocation line from a greater obstacle density in the slip plane is outweighed by the larger effect that reducing the plate diameter has on the obstacle's strength.

A complication in the above argument is that, when precipitation occurs explicitly on dislocations, the strengthening contributions from forest hardening and precipitation cannot be so simply considered in isolation. For example, there are synergistic benefits from precipitation occurring entirely on dislocations, as this will pin the dislocation forest network, which are challenging to take into account. Due to the difficulty in separating out these effects, we have also not attempted to use a more sophisticated superposition law than direct summation. As has been discussed recently by de Vaucorbeil et al., better predictions can theoretically be obtained by using a 2D areal glide approach to explicitly determine the superposition law exponents when combining strengthening terms [44]. It could therefore be argued that the good agreement seen here between the simple model used, which involved summation of the strengthening terms but minimal fitting parameters, and the alloys measured flow stress, is fortuitous.

Nevertheless, the predictions of the precipitation model (that has previously been rigorously validated [1,24]) still clearly show that in the alloy studied the strengthening contribution from precipitation hardening would be expected to reduce with higher levels of pre-strain. Thus, overall, while previous research has

attributed the higher yield strength seen in alloys like AA2195 with increased pre-strain to an increase in the number density of fine T₁ precipitates [8,13], our results reveal the opposite, in that we see a reduction in the T₁ strengthening contribution with increasing levels of pre-strain and that the progressive increase in strength that results from high levels of pre-strain is a consequence of the high level of strain hardening retained in the material owing to a low rate of recovery. This conclusion is exemplified by Fig. 15, where, for the 15% pre-stretched condition, the increase in strength estimated from strain hardening is approximately equal to that from the T₁ precipitates. In fact, at this high pre-strain level, the increase in strength from precipitation hardening is predicted to have reduced by 25%, relative to that seen for a conventional industrial stretching treatment, involving a pre-strain of 3%.

6. Conclusions

It has been demonstrated that the increase in yield strength seen in Gen3 Al–Cu–Li alloys, on stretching following solution treatment, continues to much higher pre-strain levels than are used in current industrial practice. The practical limit that can be applied, owing to plastic instability in tensile stretching the solution treated alloy, was determined to be around 15%. Nevertheless, at this pre-stretch level the yield strength of the AA2195 alloy investigated was found to increase to ~670 MPa, compared to ~590 MPa with a standard T8 temper.

XRD line broadening measurements suggested a continual increase in dislocation density with pre-strain and in the TEM a very uniform dislocation distribution was still found at high pre-strain levels. The XRD results also indicate a surprisingly low reduction in dislocation density after artificial ageing, implying that recovery is greatly inhibited in the AA2195 alloy. This has been attributed to a strong solute interaction between dislocations and the Cu and Mg in solution, as well as the strong segregation of Cu and Mg to, and the nucleation of T₁ plates on, dislocations during the early stages of artificial ageing.

Measurements from STEM images revealed a continued decrease in the T₁ plate's average diameter, as well as a narrowing of their size distribution and an increase in number density, with increasing pre-strain levels up to 15%. The spatial distribution of the T₁ phase was also found to reflect the uniform dislocation density still seen in the samples subjected to large pre-strains and this led to a reduction in the JMAK exponent (*n*) with increased pre-strain. However, the thickness of the T₁ plates remained constant (at approximately 1.3 nm) into the higher stretching range.

Good agreement was found between the experimental results and predictions of the effect of pre-stretch on the upper bound strain hardening and precipitation hardening contributions to the alloy's yield stress. It was shown that the strength contribution from precipitation hardening decreased with increasing pre-stretch, owing to the stronger dependence of the obstacle strength on the plate diameter relative to the precipitate density. In contrast, due to the low level of recovery, the contribution from strain hardening increased parabolically with pre-stretch. Thus, while previous research has attributed the increase in yield strength seen in alloys like AA2195 with increased pre-strain to an increase in the number density of T₁ precipitates, the results here suggest the opposite. In that, there is a reduction in the T₁ strengthening contribution with increasing levels of pre-strain and the increase in strength that results from high levels of pre-strain is a consequence of the high level of strain hardening retained in the material following artificial ageing.

Acknowledgements

The author would like to thank the EPSRC funded LATEST2 Programme (EP/G022402/1) and Primetals Technologies Ltd for financially supporting this project, and Constellium for the supply of materials. Particular thanks are owed to Dr. Richard Cindery for facilitating the project and providing continued encouragement and support. Thanks are also given to the technical staff at the University of Manchester who assisted in the manufacture of test pieces and in the use of laboratory equipment. In particular, thanks go to Matthew Smith for his assistance in operating the TITAN microscope. Finally, thanks go to Dr. Joao Quinta da Fonseca and Thomas Seymour for illuminating conversations regarding XRD peak broadening.

References

- [1] T. Dorin, A. Deschamps, F. De Geuser, C. Sigli, Quantification and modelling of the microstructure/strength relationship by tailoring the morphological parameters of the T₁ phase in an Al–Cu–Li alloy, *Acta Mater.* 75 (2014) 134–146.
- [2] G. Marsh, Composites and metals – a marriage of convenience? *Reinf. Plasta* 58 (2014) 38–42, [http://dx.doi.org/10.1016/S0034-3617\(14\)70108-0](http://dx.doi.org/10.1016/S0034-3617(14)70108-0).
- [3] C. Giummarrà, B. Thomas, R.J. Rioja, New aluminium lithium alloys for aerospace applications, in: *Light Met. Technol. Conf.*, Saint-Sauveur, Quebec, Canada, 2007, pp. 41–46.
- [4] R.J. Rioja, J. Liu, The evolution of Al-Li base products for aerospace and space applications, *Metall. Mater. Trans. A* 43 (2012) 3325–3337, <http://dx.doi.org/10.1007/s11661-012-1155-z>.
- [5] T. Warner, Recently developed aluminium solutions for aerospace applications, *Mater. Sci. Forum* 519–521 (2006) 1271–1278.
- [6] N. Eswara Prasad, A.A. Gokhale, R.J.H. Wanhill, *Aluminium-Lithium Alloys*, Elsevier Ltd, Oxford, 2014.
- [7] J.R. Davis, *ASM Speciality Handbook: Aluminium and Aluminium Alloys*, ASM International, Ohio, 1993.
- [8] B.M. Gable, A.W. Zhu, A.A. Csontos, E.A. Starke Jr., The role of plastic deformation on the competitive microstructural evolution and mechanical properties of a novel Al–Li–Cu–X alloy, *J. Light Met.* 1 (2001) 1–14, [http://dx.doi.org/10.1016/s1471-5317\(00\)00002-x](http://dx.doi.org/10.1016/s1471-5317(00)00002-x).
- [9] W.A. Cassada, G.J. Shiflet, E.A. Starke, The effect of plastic deformation on Al₂CuLi_x (T₁) precipitation, *Metall. Trans. A* 22 (1991) 299–306, <http://dx.doi.org/10.1007/bf02656799>.
- [10] S.P. Ringer, B.C. Muddle, I.J. Polmear, Effects of cold work on precipitation in Al–Cu–Mg–(Ag) and Al–Cu–Li–(Mg–Ag) alloys, *Metall. Mater. Trans. A* 26 (1995) 1659–1671, <http://dx.doi.org/10.1007/BF02670753>.
- [11] J.W. Martin, *Precipitation Hardening*, second ed., Butterworth-Heinemann, Oxford, 1998.
- [12] O.S. Es-Said, C.A. Bradberry, J.Y. Hassoun, R.A. Parish, A. Nash, N.C. Smythe, et al., Effect of stretch orientation and rolling orientation on the mechanical properties of 2195 Al–Cu–Li alloy, *Mater. Eng. Perform.* 20 (2010) 1171–1179.
- [13] E.W. Lee, W.E. Frazier, The effect of stretch on the microstructure and mechanical properties of 2090 Al–Li, *Scr. Metall.* 22 (1988) 53–57, [http://dx.doi.org/10.1016/s0036-9748\(88\)80305-3](http://dx.doi.org/10.1016/s0036-9748(88)80305-3).
- [14] D. Tsivoulas, P. Prangnell, Comparison of the effect of individual and combined Zr and Mn additions on the fracture behavior of Al–Cu–Li alloy AA2198 rolled sheet, *Metall. Mater. Trans. A* 45 (2014) 1338–1351, <http://dx.doi.org/10.1007/s11661-013-2103-2>.
- [15] V. Araullo-Peters, B. Gault, F. De Geuser, A. Deschamps, J. Cairney, Microstructural evolution during ageing of Al–Cu–Li–X alloys, *Acta Mater.* 66 (2014) 199–208.
- [16] H.K. Hardy, J.M. Silcock, The phase sections at 500°C and 350°C of aluminium rich aluminium–copper–lithium alloys, *J. Inst. Met.* 84 (n.d.) 423–428.
- [17] B. Noble, G.E. Thompson, T₁ (Al₂ CuLi) precipitation in aluminium–copper–lithium alloys, *Met. Sci. J.* 6 (1972) 167–174.
- [18] P. Donnadieu, Y. Shao, F. De Geuser, G.A. Botton, S. Lazar, M. Cheynet, et al., Atomic structure of T₁ precipitates in Al–Li–Cu alloys revisited with HAADF-STEM imaging and small-angle X-ray scattering, *Acta Mater.* 59 (2011) 462–472, <http://dx.doi.org/10.1016/j.actamat.2010.09.044>.
- [19] B. Decreus, A. Deschamps, F. De Geuser, P. Donnadieu, C. Sigli, M. Weyland, The influence of Cu/Li ratio on precipitation in an Al–Cu–Li–x alloys, *Acta Mater.* 61 (2013) 2207–2218.
- [20] J.C. Huang, A.J. Ardell, Strengthening mechanisms associated with T₁ particles in two Al–Li–Cu alloys, *Le. J. Phys. Colloq.* 48 (1987), <http://dx.doi.org/10.1051/jphyscol:1987343>. C3–373–C3–383.
- [21] A. Deschamps, B. Decreus, F. De Geuser, T. Dorin, M. Weyland, The influence of precipitation on plastic deformation of Al–Cu–Li alloys, *Acta Mater.* 61 (2013) 4010–4021, <http://dx.doi.org/10.1016/j.actamat.2013.03.015>.
- [22] J. Nie, B. Muddle, On the form of the age-hardening response in high strength aluminium alloys, *Mater. Sci. Eng. A* 319–321 (2001) 448–451, [http://dx.doi.org/10.1016/S0921-5093\(01\)01054-1](http://dx.doi.org/10.1016/S0921-5093(01)01054-1).
- [23] A.A. Csontos, E.A. Starke, The effect of inhomogeneous plastic deformation on

- the ductility and fracture behavior of age hardenable aluminum alloys, *Int. J. Plast.* 21 (2005) 1097–1118, <http://dx.doi.org/10.1016/j.ijplas.2004.03.003>.
- [24] J.F. Nie, B.C. Muddle, Microstructural design of high-strength aluminum alloys, *J. Phase Equilibria*, 19 (1998) 543–551.
- [25] F.J. Humphreys, M. Hatherly, *Recrystallisation and Related Annealing Phenomena*, second ed., Elsevier Ltd, Oxford, 2004.
- [26] B.S. BSI, EN ISO 6892-1 Metallic Materials - Tensile Testing, Test Piece, 2009.
- [27] T. Ungar, A. Borbely, The effect of dislocation contrast on x-ray line broadening: a new approach to line profile analysis, *Appl. Phys. Lett.* 69 (1996) 3173–3175.
- [28] M. Wojdyr, Fityk: A General-Purpose Peak Fitting Program, *J. Appl. Crystallogr.* 43 (2010) 1126–1128.
- [29] T. Dorin, A. Deschamps, F. Gueser, M. Weyland, Quantitative description of the T1 morphology and strengthening mechanisms in an age-hardenable Al–Li–Cu alloy, in: 13th Int. Conf. Alum. Alloy, 2012, pp. 1155–1160.
- [30] T. Dorin, A. Deschamps, F. De Geuser, W. Lefebvre, C. Sigli, Quantitative description of the T1 formation kinetics in an Al–Cu–Li Alloy using differential scanning calorimetry, small-angle X-ray scattering and transmission electron microscopy, *Philos. Mag.* 94 (2014) 1012–1030.
- [31] M. Avrami, Kinetics of phase change. I: general theory, *J. Chem. Phys.* 7 (1939) 1103–1112. <http://www.scopus.com/inward/record.url?eid=2-s2.0-0342869049&partnerID=tZotx3y1>. <http://www.scopus.com/inward/record.url?eid=2-s2.0-0342869049&partnerID=tZotx3y1>.
- [32] C.E. Feltrin, Dislocation arrangements in aluminium deformed by repeated tensile stresses, *Acta Metall.* 2 (1963) 817–828.
- [33] N.Y. Zolotorevsky, A.N. Solonin, A.Y. Churymov, V.S. Zolotorevsky, Study of work hardening of quenched and naturally aged Al–Mg and Al–Cu alloys, *Mater. Sci. Eng. A* 502 (2009) 111–117, <http://dx.doi.org/10.1016/j.msea.2008.10.010>.
- [34] T. Ungar, Dislocation densities, arrangements and character from X-ray diffraction experiments, *Mater. Sci. Eng. A* (2001) 14–22.
- [35] T. Ungar, Microstructural parameters from X-ray diffraction peak broadening, *Scr. Mater.* 51 (2004) 777–781.
- [36] T. Ungar, Strain broadening caused by dislocations, in: Denver X-Ray Conf., International Centre for Diffraction Data, 1997.
- [37] T. Ungar, G. Tichy, Peak broadening anisotropy in deformed face-centred-cubic and hexagonal close-packed alloys, *Phys. Status Solidi A* 171 (1999) 425–434.
- [38] T. Ungar, I. Dragomir, A. Revesz, A. Borbely, The contrast factors of dislocations in cubic crystals: the dislocation model of strain anisotropy in practice, *J. Appl. Crystallogr.* 32 (1999) 992–1002.
- [39] T.H. Simm, P.J. Withers, J. Quinta Da Fonseca, Peak broadening anisotropy in deformed face-centred-cubic and hexagonal close-packed alloys, *J. Appl. Crystallogr.* 47 (2014) 1535–1551.
- [40] A. Borbely, J. Dragomir-Cernescu, G. Ribárik, T. Ungár, Computer program ANIZC for the calculation of diffraction contrast factors of dislocations in elastically anisotropic cubic, hexagonal and trigonal crystals, *J. Appl. Crystallogr.* 36 (2003) 160–162, <http://dx.doi.org/10.1107/S0021889802021581>.
- [41] S.K. Rai, A. Kumar, V. Shankar, T. Jayakumar, K. Bhanu Sankara Rao, B. Raj, Characterization of microstructures in Inconel 625 using X-ray diffraction peak broadening and lattice parameter measurements, *Scr. Mater.* 51 (2004) 59–63, <http://dx.doi.org/10.1016/j.scriptamat.2004.03.017>.
- [42] D.A. Porter, K.E. Easterling, M.Y. Sherif, *Phase Transformations in Metals and Alloys*, third ed., CRC Press, 2009.
- [43] J.W. Christian, *The Theory of Transformations in Metals and Alloys*, third ed., Pergamon, 2002.
- [44] A. de Vaucozelbeil, W.J. Poole, C.W. Sinclair, The superposition of strengthening contributions in engineering alloys, *Mater. Sci. Eng. A* 582 (2013) 147–154, <http://dx.doi.org/10.1016/j.msea.2013.06.032>.
- [45] H.R. Sherriff, M.F. Ashby, A process model for age hardening of aluminium alloys—I. The model, *Acta Metall. Mater.* 38 (1990) 1789–1802, [http://dx.doi.org/10.1016/0956-7151\(90\)90291-N](http://dx.doi.org/10.1016/0956-7151(90)90291-N).
- [46] O. Myhr, Modelling of the age hardening behaviour of Al–Mg–Si alloys, *Acta Mater.* 49 (2001) 65–75, [http://dx.doi.org/10.1016/S1359-6454\(00\)00301-3](http://dx.doi.org/10.1016/S1359-6454(00)00301-3).
- [47] D. Bardel, M. Perez, D. Nelias, A. Deschamps, C.R. Hutchinson, D. Maisonneuve, et al., Coupled precipitation and yield strength modelling for non-isothermal treatments of a 6061 aluminium alloy, *Acta Mater.* 62 (2014) 129–140, <http://dx.doi.org/10.1016/j.actamat.2013.09.041>.
- [48] M.J. Starink, A. Deschamps, S.C. Wang, The strength of friction stir welded and friction stir processed aluminium alloys, *Scr. Mater.* 58 (2008) 377–382, <http://dx.doi.org/10.1016/j.scriptamat.2007.09.061>.
- [49] M.J. Starink, S.C. Wang, A model for the yield strength of overaged Al–Zn–Mg–Cu alloys, *Acta Mater.* 51 (2003) 5131–5150, [http://dx.doi.org/10.1016/S1359-6454\(03\)00363-X](http://dx.doi.org/10.1016/S1359-6454(03)00363-X).
- [50] J. da Costa Teixeira, D.G. Cram, L. Bourgeois, T.J. Bastow, A.J. Hill, C.R. Hutchinson, On the Strengthening response of aluminum alloys containing shear-resistant plate-shaped precipitates, *Acta Mater.* 56 (2008) 6109–6122.
- [51] K.M. Nairn, B.M. Gable, R. Stark, N. Ciccosillo, A.J. Hill, B.C. Muddle, et al., Monitoring the evolution of the matrix copper composition in age hardenable Al–Cu alloys, *Mater. Sci. Forum* 519–521 (2006) 591–596.
- [52] J.M. Fragomeni, B.M. Hillberry, Determining the effect of microstructure and heat treatment on the mechanical strengthening behavior of an aluminum alloy containing lithium precipitation hardened with the Al₃Li intermetallic phase, *J. Mater. Eng. Perform.* 9 (2000) 428–440.
- [53] Z.B. Jiao, J.H. Luan, Z.W. Zhang, M.K. Miller, C.T. Liu, High-strength steels hardened mainly by nanoscale NiAl precipitates, *Scr. Mater.* 87 (2014) 45–48, <http://dx.doi.org/10.1016/j.scriptamat.2014.05.006>.
- [54] Y. Huang, J.D. Robson, P.B. Prangnell, The formation of nanograin structures and accelerated room-temperature theta precipitation in a severely deformed Al–4 wt.% Cu alloy, *Acta Mater.* 58 (2010) 1643–1657, <http://dx.doi.org/10.1016/j.actamat.2009.11.008>.
- [55] R. Madec, B. Devincre, L.P. Kubin, From dislocation junctions to forest hardening, *Phys. Rev. Lett.* 89 (2002) 255508.
- [56] W.J. Poole, J.A. Saeter, S. Skjervold, G. Waterloo, A model for predicting the effect of deformation after solution treatment on the subsequent artificial ageing behavior of AA7030 and AA7108 alloys, *Metall. Mater. Trans. A* 31A (2000) 2327–2338.
- [57] D.A. Hughes, Microstructural evolution in a non-cell forming metal: Al–Mg, *Acta Metall. Mater.* 41 (1993) 1421–1430, [http://dx.doi.org/10.1016/0956-7151\(93\)90251-M](http://dx.doi.org/10.1016/0956-7151(93)90251-M).
- [58] E. Nes, K. Marthinsen, Modeling the evolution in microstructure and properties during plastic deformation of F.C.C. – metals and alloys – an approach towards a unified model, *Mater. Sci. Eng. A* 322 (2002) 176–193, [http://dx.doi.org/10.1016/S0921-5093\(01\)01130-3](http://dx.doi.org/10.1016/S0921-5093(01)01130-3).
- [59] T. Schulthess, P.E. Turchi, A. Gonis, T.-G. Nieh, Systematic study of stacking fault energies of random Al-based alloys, *Acta Mater.* 46 (1998) 2215–2221, [http://dx.doi.org/10.1016/S1359-6454\(97\)00432-1](http://dx.doi.org/10.1016/S1359-6454(97)00432-1).
- [60] W.A. Cassada, G.J. Shifflet, E.A. Starke, Mechanism of Al₂CuLi (T1) nucleation and growth, *Metall. Trans. A* 22A (1991) 287–297.
- [61] B. Noble, G.E. Thompson, Precipitation characteristics of aluminium-lithium alloys containing magnesium, *J. Inst. Met.* 101 (1973) 111–115.
- [62] T. Dorin, F. De Geuser, W. Lefebvre, C. Sigli, A. Deschamps, Strengthening mechanisms of T1 precipitates and their influence on the plasticity of an Al–Cu–Li alloy, *Mater. Sci. Eng. A* 605 (2014) 119–126, <http://dx.doi.org/10.1016/j.msea.2014.03.024>.